We are IntechOpen, the world's leading publisher of Open Access books Built by scientists, for scientists

4,800
Open access books available

122,000
International authors and editors

135M
Downloads

Our authors are among the

154
Countries delivered to

TOP 1%
most cited scientists

12.2%
Contributors from top 500 universities

WEB OF SCIENCE™

Selection of our books indexed in the Book Citation Index in Web of Science™ Core Collection (BKCI)

Interested in publishing with us?
Contact book.department@intechopen.com

Numbers displayed above are based on latest data collected.
For more information visit www.intechopen.com

17

Protons Acceleration by CO_2 Laser Pulses and Perspectives for Medical Applications

Pasquale Londrillo, Graziano Servizi, Andrea Sgattoni, Stefano Sinigardi, Marco Sumini and Giorgio Turchetti
Università di Bologna, INFN Sezione di Bologna
Italy

1. Introduction

The acceleration of electrons with the high electric fields generated in a plasma by a very intense laser pulse was proposed over forty years ago [Tajima & Dawson (1979)], but only the advent of the chirped pulse amplification CPA [Mourou et al. (2006)] allowed to increase the laser power and intensity up to the required values. The continuous progress, since a decade, of compact Ti:Sa lasers allowed 1 GeV good quality electron beams to be generated [Leemans et al. (2006)]. The optical acceleration of protons and ions has been also actively investigated. The highest energy of protons, 60 MeV, has been reached with short high energy pulses of Nd:Yag lasers, developed for inertial fusion [Snavely (2000)]. With compact ultrashort Ti:Sa laser pulses intensities of 10^{21} W/cm^2 are reached and proton beams with energy up to a few tens of MeV are obtained [Zeil et al. (2010)].

The targets are typically thin metal foils and the acceleration is achieved in the TNSA regime (Target Normal Sheath Acceleration). The laser, interacting with an overcritical plasma, cannot propagate through it and heats the electrons on the surface of the target. A large number of "hot" electrons is hence produced and they are are accelerated in the forward direction and can cross the target. When reaching the rear surface they create an intense electrostatic field which accelerates the protons present on the surface [Passoni & Lontano (2004)]. The energy spectrum is exponential and the angular spread is significant so that the beam is not suitable for free propagation. Energy selection and collimation may reduce the intensity below the threshold required for any application. However other acceleration mechanisms have been considered such as the radiation pressure dominated regime RPA (Radiation Pressure Acceleration), where two distinct mechanism act depending on the thickness h of the target. If $h \sim \lambda$ the hole boring regime with break-up of the electron density wave is active [Macchi et al. (2005)], whereas for ultrathin targets the acceleration mechanism is the same as for the relativistic mirror [Londrillo et al. (2010); Macchi et al. (2009)] and high efficiencies can be reached. This regime was recently experimentally observed using a few nanometers carbon targets, a circularly polarized laser pulse with $\lambda \sim 1\mu$m and very high contrast [Henig (2009)].

The efficiency of the RPA should be higher than TNSA and the proton bunches should have a small energy and angular spread; however the requirements of circular polarization and high contrast of the laser pulse render this regime not easily achievable. The subcritical or

quasi-critical targets are also a possible alternative because the laser-plasma energy coupling can be very high with a much higher energy transfer from the laser pulse to the plasma: a different regime may be achieved where the laser drills a channel and a strong electron current is created on its trail. At the exit from the plasma it creates a magnetic azimuthal field and a longitudinal electric field. As a consequence, the protons are efficiently accelerated and nicely collimated [Bulanov (2010); Nakamura, Bulanov, Esirkepov & Kando (2010); Naumova & Bulanov (2002); Yogo (2008)]. Experimental results with near critical targets confirmed the theoretical and simulation results on the enhancement of maximum energy and reduction of angular spread with respect to the TNSA acceleration mechanism [Fukuda & Bulanov (2009)].

The possibility of reaching energies close to the threshold of 60 MeV for cancer therapy with compact Ti:Sa laser system has stimulated several projects dedicated to medical applications. Indeed the protons or ions deposit most of their energy at the end of their range and are biologically more effective with respect to electrons or X rays since they allow to spare nearby healthy tissues. However the cyclotrons and synchrotrons currently used require large and expensive infrastructures. The use of laser acceleration opens a perspective for more compact and cheaper devices suitable to be installed on a regional scale. Two possible strategies are being considered:

A) increase the power of the laser system in order to reach energies in the 100-200 MeV energy range [Bulanov (2008); Hofmann (2011); Murakami (2008)]

B) use the laser system as injector into a DTL linac to increase the energy starting from 10 MeV [Antici (2011)] or to inject a 30 MeV laser accelerated protons bunch, into a high field compact linac in order to raise the energy up to 100 or 200 MeV [Londrillo et al. (2011)].

The hybrid acceleration scheme does not require to develop new laser systems but only the improvement of targets and the design of a transport system capable of shaping the beam in such a way to render it suitable for injection. Simulations and experiments are presently being developed to explore the feasibility of transport of an optically accelerated protons bunch reaching the beam quality required for irradiation and for injection into a post-acceleration device [Melone (2011); Nishiuchi (2010); Schollmeier (2008)]. The reduction of the energy spread with a longitudinal phase space rotation provided by a synchronized RF was also proved [Noda (2008)].

Recently, new protons acceleration experiments have been performed taking advantage of short pulses of long wavelength $\lambda = 10\mu$m produced by CO_2 lasers. This approach provides a parallel research pathway which offers some advantages. Being the wavelength one order of magnitude larger than the optical values typical of Ti:Sa or Nd laser, the plasma critical density for $\lambda = 10\mu$m is about 10^{19} cm^{-3} which can be reached ionizing a supersonic gas-jet. The CO_2 lasers deliver a pulse with a native quasi circular polarization which is interesting for triggering the RPA regime at lower intensities.

Recent experiments showed that using a 1 TW pulse of 1 J interacting with a solid target, protons can be accelerated up to 1 MeV with exponential energy spectrum and wide angular spread typical of TNSA regime [Pogorelsky (2010b)]. On a gas jet at the critical density a quasi monochromatic beam of protons at 2 MeV was obtained suggesting that a RPA mechanism is dominating [Pogorelsky (2010a)]. With a train of short pulses and 100 J total energy a different acceleration mechanism was achieved and protons of 25 MeV, even though a low

number, were accelerated with a very small energy spread [Haberberger, Tochitsky, Fiuza, Gong, Fonseca, Silva, Mori & Joshi (2011); Haberberger, Tochitsky, Gong & Joshi (2011)]. This result inserts the CO_2 lasers among the possible candidates for the production of proton beams for medical therapy, possibly combined with a post acceleration device. The CO_2 lasers have high efficiency and produce almost circularly polarized light which is suited for acceleration mechanisms like RPA. In particular the possibility of using gas jets at under-critical or slightly overcritical density opens very interesting perspectives because of the high repetition rate allowed, the absence of debris (opposed to the case of solid thin targets) jointly with the advantages of circular polarization.

We can now study the very same physical problem using a CO_2 laser instead of a Ti:Sa laser keeping the dynamics of the interaction unchanged. This can be done keeping unchanged the adimensional parameters which characterize the laser-plasma: the ratio of the plasma density over critical density (n/n_c) and the normalized vector potential (a). This correspond to consider a CO_2 laser pulse with the same peak power but ten times longer (same number of wave cycle) and a laser waist proportional to the wavelength. The plasma density is hundred times lower and the total volume interested by the acceleration is three order of magnitude larger than the case of a Ti:Sa laser. If we assume a definite fraction of the protons in the corresponding volume are accelerated and the density is kept at the critical value, then the number of accelerated protons is proportional to λ. If coupled with a high repetition rate, long wavelength pulses may offer a further advantage to reach the doses required by therapy.

In the present note we shall review the basic mechanisms for laser acceleration to present the related scaling laws and compare the results one expects from small (1 μ) and large (10 μ) wavelength pulses. Systematic 2D and 3D simulations were performed with the high order PIC code `ALaDyn` [Benedetti et al. (2008)] developed by the university of Bologna to provide quantitative results in addition to the qualitative results of scaling laws. We shall also discuss the transport of a protons beam through an optical system.

The paper consists of six sections: after this introduction, in section 2 we recall the basic features and parameters of the laser beam, in section 3 the TNSA regime is reviewed, in section 4 the RPA regime is presented, in section 5 the acceleration on under-critical target is discussed, in section 6 we discuss the transport of the optically accelerated proton bunch, in section 7 we analyze the perspectives for therapy.

2. Laser beam interaction with matter

A laser pulse is described by an electromagnetic wave packet, which is a solution of Maxwell's equations

$$\begin{aligned} \mathrm{rot}\,\mathbf{E} &= -\frac{1}{c}\frac{\partial}{\partial t}\mathbf{B} & \mathrm{div}\,\mathbf{B} &= 0 \\ \mathrm{rot}\,\mathbf{B} &= \frac{4\pi}{c}\mathbf{j} + \frac{1}{c}\frac{\partial}{\partial t}\mathbf{E} & \mathrm{div}\,\mathbf{E} &= 4\pi\rho \end{aligned} \tag{1}$$

in the vacuum where source charges and currents are absent $\rho = 0$, $\mathbf{j} = 0$. The sources arise when the pulse propagates in material medium creating a plasma. The scalar and vector

potential defined by

$$\mathbf{B} = \text{rot}\,\mathbf{A} \qquad\qquad \mathbf{E} = -\text{grad}\,\Phi - \frac{1}{c}\frac{\partial}{\partial t}\mathbf{A} \tag{2}$$

identically satisfy he first two equations. Choosing a gauge such that

$$\text{div}\,\mathbf{A} + \frac{1}{c}\Phi = 0 \tag{3}$$

the last two equations become the wave equations

$$\begin{aligned} \Delta\mathbf{A} - \frac{1}{c^2}\frac{\partial^2}{\partial t^2}\mathbf{A} &= -\frac{4\pi}{c}\mathbf{j} \\ \Delta\Phi - \frac{1}{c^2}\frac{\partial^2}{\partial t^2}\Phi &= -4\pi\rho \end{aligned} \tag{4}$$

In the vacuum $\rho = 0$ and we may choose $\Phi = 0$. The gauge equation in this case reads div $\mathbf{A} = 0$ and the electric field is given by $\mathbf{E} = -c^{-1}\partial\mathbf{A}/\partial t$. If we consider a two dimensional wave propagating in the x, z plane we may set $A_x = \partial A/\partial z$ and $A_z = -\partial A/\partial x$ where $A = A(x, z)$ so that div $\mathbf{A} = 0$ is identically satisfied. In this case the electric field is given by

$$E_x = -\frac{1}{c}\frac{\partial}{\partial t}\frac{\partial}{\partial z}A \qquad E_y = 0 \qquad E_z = \frac{1}{c}\frac{\partial}{\partial t}\frac{\partial}{\partial x}A \tag{5}$$

and the magnetic field

$$B_x = 0 \qquad B_y = \left(\frac{\partial^2}{\partial x^2} + \frac{\partial^2}{\partial z^2}\right)A \qquad B_z = 0 \tag{6}$$

Given an initial Gaussian wave field specified by

$$A(x, z, 0) = A_0(x, z) \equiv \frac{e^{-x^2/2\sigma_x^2}}{\sqrt{2\pi\sigma_x^2}}\frac{e^{-z^2/2\sigma_z^2}}{\sqrt{2\pi\sigma_z^2}}\cos(k_0\, z) \tag{7}$$

The evolution at time t is obtained by computing its Fourier transform and by taking into account that A satisfies the wave equation

$$\Delta A - \frac{1}{c^2}\frac{\partial^2}{\partial t^2}A = 0 \tag{8}$$

The result for the propagating wave packet is given by

$$A(x, z, t) = \frac{1}{(2\pi)^2}\int_{-\infty}^{+\infty} dk_x \int_{-\infty}^{+\infty} dk_z\, e^{-\sigma_x^2 k_x^2/2}\, e^{-\sigma_z^2 (k_z - k_0)^2/2}\cos(xk_x + zk_z - \omega t) \tag{9}$$

When the wave interacts with a medium it ionizes it if the intensity is sufficiently high and the charged particles move according to the equations of motion

$$\frac{d\mathbf{r}}{dt} = \frac{\mathbf{p}}{m\gamma} \qquad\qquad \frac{d\mathbf{p}}{dt} = e\mathbf{E} + \frac{e}{mc\gamma}\,\mathbf{p}\times\mathbf{B} \tag{10}$$

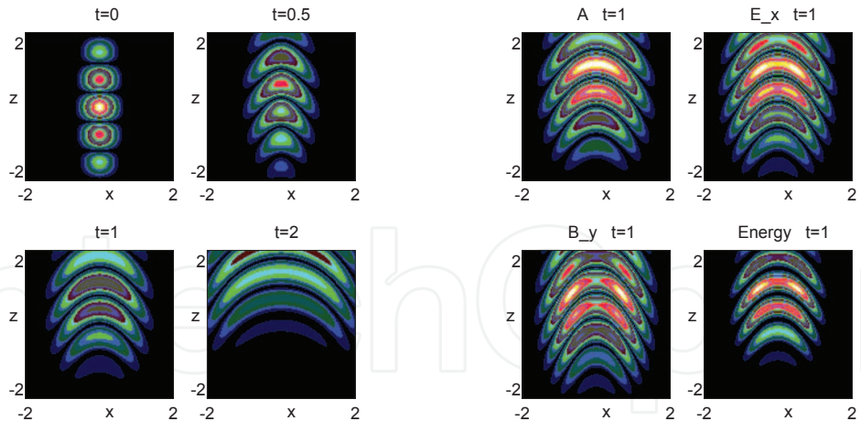

Fig. 1. Gaussian wave packet for the function A defined by eq. (7, 9), for $\sigma_x = 0.25$, $\sigma_z = 1$, $k_0 = 4$, $c = 1$, at different times (left figures). Electric field E_x, magnetic field B_y and energy at time $t = 1$ (right figures).

where e is the electric charge and γ is the relativistic factor

$$\gamma = \left(1 + \frac{\mathbf{p}^2}{m^2c^2}\right)^{1/2}$$

Given N particles we introduce the phase space density $f(\mathbf{r}, \mathbf{p}, t)$, which evolves according to the Liouville equation

$$\frac{\partial f}{\partial t} + \frac{\mathbf{p}}{m\gamma}\,\frac{\partial f}{\partial \mathbf{r}} + \left(e\mathbf{E} + \frac{e}{mc\gamma}\,\mathbf{p}\times\mathbf{B}\right)\,\frac{\partial f}{\partial \mathbf{p}} = 0 \tag{11}$$

where the fields are solution of the Maxwell's equations, the sources being defined by

$$\rho(\mathbf{r}, t) = e\int f(\mathbf{r}, \mathbf{p}, t)\; d\mathbf{p} \qquad\qquad \mathbf{j} = e\int \frac{\mathbf{p}}{m\gamma}\, f(\mathbf{r}, \mathbf{p}, t)\; d\mathbf{p} \tag{12}$$

The set (1), (11), (12) forms the Maxwell-Vlasov equations and provides the dynamical setting to investigate the laser plasma interaction. In actual computations the number N of numerical particles, used to sample the phase space density, is considerably lower than the number $N_{\rm ph}$ of physical particles and the masses and charges are $N_{\rm ph}/N$ times larger with respect to the masses and charges of the physical particles.The equations of motion are not affected since they depend only on the ratio e/m. The computation of charge densities and currents requires an interpolation procedure with smooth functions like splines,

2.1 Basic parameters

The basic parameter of the electromagnetic wave is a dimensionless quantity which gives the ratio between the electromagnetic energy and the electron (or proton) rest mass energy

$$a = \frac{eA}{mc^2} \qquad\qquad a_p = \frac{eA}{m_pc^2} \tag{13}$$

When $a \sim 1$ the electron becomes relativistic since the energy acquired from the wave is comparable with its rest energy. The intensity is related to the electromagnetic energy by

$$\frac{I}{c} = \frac{B^2 + E^2}{8\pi} = \pi \frac{A^2}{\lambda^2} \tag{14}$$

and consequently letting $r_c = e^2/(mc^2) = 3\,10^{-13}$ cm be the classical electron radius we have

$$a^2 = \frac{r_c}{\pi\, mc^3}\, \lambda^2 I = \frac{I}{mc^3 n_c} \tag{15}$$

where n_c is the critical density defined below (19). A frequently used formula follows

$$a = 0.85\ 10^{-9} I^{1/2}(\mathrm{W/cm^2})\, \lambda(\mu\mathrm{m}) \tag{16}$$

The most relevant plasma parameter is the electron density which determines the plasma oscillations frequency ω_p

$$\omega_p^2 = \frac{4\pi e^2 n}{m} = 4\pi r_c c^2 n \tag{17}$$

where $n = \rho/e$ is the electron density, and ρ is the charge density. The plasma is an active optical medium and its refraction index is

$$n_{\mathrm{refr}} = \left(1 - \frac{\omega_p^2}{\omega^2}\right)^{1/2} \tag{18}$$

For $\omega_p < \omega$ the medium is transparent. The density n_c at which the medium becomes opaque is called critical density and is given by $\omega_p = \omega$ namely

$$n_c = \frac{\omega^2}{4\pi c^2 r_c} \simeq \frac{\pi}{\lambda^2 r_c} = \frac{10^{21}}{\lambda^2(\mu\mathrm{m})}\ \mathrm{cm}^{-3} \tag{19}$$

When the plasma is overcritical the wave becomes evanescent and decays exponentially. The decay length, called skin depth, is given by

$$\ell_s = \frac{\lambda}{2\pi}\left(\frac{\omega_p^2}{\omega^2} - 1\right)^{-1/2} = \frac{\lambda}{2\pi}\left(\frac{n}{n_c} - 1\right)^{-1/2} \tag{20}$$

If we assume the waist to be a fixed multiple of the wavelength, $w = \kappa\lambda$ then a^2 is proportional to the pulse power and does not depend on the wavelength. On the contrary the critical density in proportional to λ^{-2}, and is $n_c = 10^{-19}$ cm^{-3} for a CO_2 laser pulse. This means that a gas jet, from which a plasma density in the range of $10^{18} \div 10^{20}$ cm^{-3} can be obtained, provides a medium with quasi critical electron density. Moreover since the pulse length is in the range of hundreds of microns, the millimetric thickness of a gas jet is adequate for protons acceleration. Since the pulse durations for a Ti:Sa and CO_2 laser are 30 fs and 1 ps respectively, in order to have the same power the ratio of the energies must be 1/30. For the same power and the same value of a, the proton energy should be the same but their number would be higher for a CO_2 pulse.

3. The TNSA regime

This regime is observed when the laser beam interacts with a metallic foil whose electron density is largely overcritical $n \gg n_c$, the thickness h of the foil is large with respect to the skin depth $h \gg \ell_s$ and the polarization is linear. When the laser pulse interacts with the overcritical plasma it is reflected by the target. A sizable fraction of its energy can be absorbed by the electrons of the plasma by linear or nonlinear mechanisms. These electrons can travel through the target and expand around both the front and the rear side. The thickness of the electron cloud is estimated equal to some Debye lengths λ_D where $\lambda_D^2 = k_B\Theta/(4\pi e^2 n)$ and Θ refers to the temperature of the electrons whose density is n. The protons which are present on both surfaces as part of the contaminants deposited on the target (hydrocarbons, water vapors) are accelerated by the electrostatic field built up by the expanding electron cloud preferentially along the normal to the surfaces. If the laser contrast is high enough the front side of the target may be preserved intact until the main part of the pulse interacts with the plasma and a substantially symmetric acceleration takes place in both forward direction (from the rear side) and backward direction (protons from the front side). On the other hand, if the front surface is destroyed by the prepulses or by the laser pedestal, only the forward acceleration is observed.

We can consider the motion of a single electron in a plane e.m. wave. Assuming that the propagation is along the z axis and the vector potential has only the A_y component, defining $a = eA_y/(mc^2)$ the generalized momenta are $P_x = 0$, $P_y = p_y - mca$, $P_z = p$. If we have a particle in an external field then $P_y = 0$ because it is so initially and it is conserved. When collective effects are present we consider a fluid approximation assuming that $\langle P_y \rangle = 0$ which implies $\langle p_y \rangle = mca$. The longitudinal motion is a coherent one given by the ponderomotive force, whereas the transverse one is random and we may assume the temperature Θ to be given by

$$k_B\Theta = T = mc^2[(1+a^2)^{1/2} - 1] \tag{21}$$

so that for $a \gg 1$ we have $k_b\Theta \simeq a\, mc^2$. As a consequence the Debye length λ_D is given by

$$\lambda_D^2 = \frac{k_B\Theta}{mc^2}\,\frac{1}{4\pi\, r_c\, n} = \frac{a}{4\pi\, r_c\, n} \tag{22}$$

where n_0 denotes the electron density. An estimate of the electrostatic field is obtained by supposing the electrons charge distribution obeys Boltzmann statistics so that $n = n_0\, e^{eV/(k_B\Theta)}$ and V satisfies the Poisson-Boltzmann equation

$$\frac{d^2V}{dz^2} = 4\pi\, n_0\, e\, \exp\left(eV/(k_B\Theta)\right) \tag{23}$$

which must be solved with the conditions $V(h) = V'(h) = 0$. The solution is given by

$$V = \frac{T}{e}\log\left(1 + \tan^2\left(\frac{h-z}{\lambda_D\sqrt{2}}\right)\right) \tag{24}$$

The longitudinal electric field is given by $E_z = -V'(z)$; the maximum protons energy $E_{\max}$ is simply the potential energy at the origin and can be expressed as

$$E_{\max}(\mathrm{MeV}) = \frac{E_{\max}}{2mc^2} \simeq \frac{a}{2}\log\left(1+\tan^2\sqrt{2}\right) \simeq 2a \tag{25}$$

This result is compatible with experiments which show a linear dependence of $E_{\max}$ with $I^{1/2}$. However for very short and very collimated laser pulses the experimentally observed scaling law is $E_{\max} \propto I^{0.8}$. More refined theoretical models agree with this scaling law [Zani et al. (2011)].

The efficiency of TNSA acceleration can be enhanced if the efficiency of the energy transfer from laser to the target can be increased. If the laser interacts with a near critical density plasma the energy coupling of the laser with the target is considerably increased, comparing with the case of highly overcritical plasma, and a higher number of "hot" electrons can be obtained. The pre-pulse induced ionization creates a pre-plasma and improves the energy transfer from the laser to the electrons letting the laser interact with a plasma at lower density. The characteristics of the preplasma are not easily controlled in a metallic target being the control of the laser-pedestal and pre-pulses very difficult. However a different design of the target may be considered where a foam layer is deposited on the thin metal foil [Nakamura, Tampo, Kodama, Bulanov & Kando (2010)]. Such a target leads to a considerably greater laser energy absorption and to possibly an improved control of the laser target interaction. Systematic 2D and 3D PIC simulations have shown that the presence of a foam increases the maximum protons energy..

In figure 2 we show a comparison of the results obtained from a fully 3D simulation of the interaction of a laser beam with $a = 10$ with a thin metal foil with and without the coating of a slightly overcritical foam layer. The saturation of the maximum energy in the considered time interval is quite evident and the gain with the foam layer is almost a factor 3.

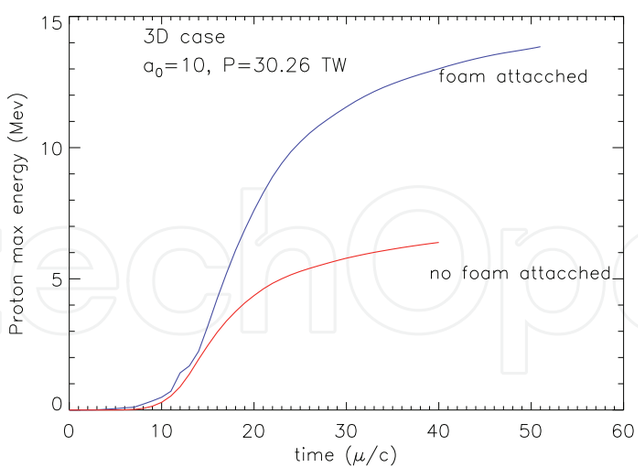

Fig. 2. Comparison of the maximum proton energy rise with time for a metal foil (red curve) with a foil on which a foam is superimposed (blue). The laser pulse has $\lambda = 0.8\,\mu$m, its duration is 25 fs, the waist is 3 μm and the power is $W = 30$ TW so that $a_0 = 10$. The foil is $0,5\,\mu$m thick with a $n = 40\,n_c$ whereas the foam layer is 2μ thick and $n = 2n_c$. The polarization is linear and the incidence is normal. The accelerated protons come form the contaminants layer which is modeled as an ultra-thin H layer of 50 nm at density $n = 9n_c$.

The main feature of TNSA is that the energy spectrum has an exponential decay with a clear cut-off. Letting $N(E)$ be the number of protons having energy in the range $[0, E]$ the spectrum is given by

$$\frac{dN}{dE} = \frac{N_0}{E_0}\, e^{-E/E_0} \quad 0 \leq E < E_{\max} \qquad \frac{dN}{dE} = 0 \quad E > E_{\max} \tag{26}$$

where $E_{\max}$ is the maximum energy where the exponential distribution is cut off. If $E_0 \ll E_{\max}$, so that the error in normalization while replacing the integration upper bound $E_{\max}$ with ∞ is negligible, then E_0 is precisely the average energy and N_0 is the total protons number. For instance suppose we have $E_{\max} = 20$ MeV and and $E_0 = 2$ MeV with $N_0 = 10^{12}$. Such a number would be obtained with a 6 J pulse if 0.3 J are transferred to the protons. We should notice that the number of protons with a narrow energy in the range $[E, E + \Delta E]$ would be

$$N([E, E + \Delta E]) \simeq N_0 \frac{\Delta E}{E_0}\, e^{-E/E_0} \tag{27}$$

and consequently choosing $E = 10$ MeV, $\Delta E = 0.1$ MeV we would have $N = 3\,10^8$ protons. The angular spread of the protons is important, so that after collimation with an iris in order to allow focusing with a quadrupole or a solenoid the number would be further reduced, possibly below 10^7, which is rather low (but might be acceptable) in view of possible applications.

In figure 3 we show the energy spectrum for a metal foil and a foam layer whose parameters are the same as in figure 2. The maximum energy is $E_{\max} \simeq 14$ MeV and the average energy is 1.8 MeV.

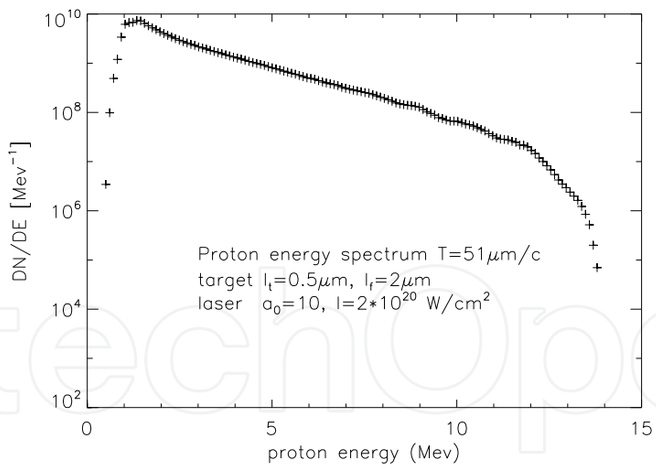

Fig. 3. Energy spectrum for metal foil with foam and the same parameters and the same laser pulse as figure 2.

In figure 4 we show the scaling of the maximum energy and average energy at different a. In this case, the average E is not computed on all the particles, but instead only on a subset that linearly fits the logarithmic plot, where the beginning and the end of the spectrum are excluded. It turns out that the average energy, in 3D simulations, is $\sim 1/7$ of the maximum energy, both for the bare target and a target with a foam.

We noticed that a good linear fit holds in both cases and that for 2D simulations the maximum value of energy $E_{\max}$ is about twice the energy obtained for 3D simulations.

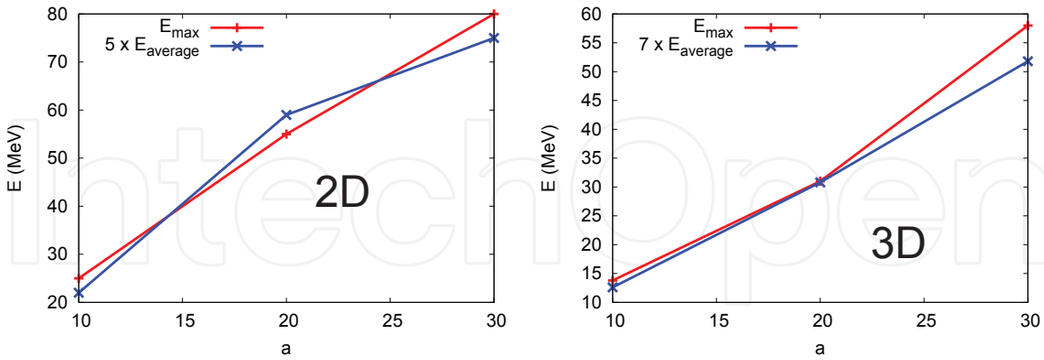

Fig. 4. Scalings for the maximum and average energies computed from linear fit on a logarithmic plot for 2D and 3D simulations for a target with a metal foil 0.5 μm thick and density $n = 80n_c$, a foam layer of 2 μm and density $n = 2n_c$, a layer of contaminants of 50 nm and density of $n = 9n_c$.

3.1 CO_2 results

Experiments in Brookhaven with 1 TW CO_2 laser pulses have shown that protons with maximum energy of 1 MeV can be obtained [Pogorelsky (2010b)]. The scaling laws obtained from both experiments and theoretical/numerical work does not offer significant perspectives to reach proton energies interesting for hadron therapy purposes unless powers in the PW range can be reached. As a consequence TNSA accelerated protons might be proposed for medical applications only coupled with a post acceleration device. Even in this case energies above 10 MeV should be reached. The use of targets with a coating of of 5-10 microns of a silicon foam with near critical density on the illuminated surface may increase the maximum energy by a significant factor (2-4) as simulations and experiments have shown [Nakamura, Tampo, Kodama, Bulanov & Kando (2010)]. As a consequence the injection energy may be reached with compact lasers. This improved type of targets may be used for CO_2 laser pulses as well. The most promising scenarios however are met when quasi critical are used, typically provided by a gas jet. In this case however we face a different acceleration regime which is dominated by the radiation pressure if the electron heating is modest as in the case of a circular polarization.

4. The RPA regime

The radiation pressure becomes the dominant mechanism in the acceleration of protons when $I > 10^{23}$ W/cm^2. However the effect of radiation pressure prevails over electrostatic acceleration even at lower energies when the electrons heating is decreased using a circularly polarized light. Given a vector potential $\mathbf{A}$ the relativistic Hamiltonian of a charged particle is

$$H = mc^2(\gamma - 1) \qquad \gamma = \left(1 + \frac{\mathbf{p}^2}{m^2c^2}\right)^{1/2} \qquad \mathbf{p} = \mathbf{P} - \frac{e}{c}\mathbf{A} \tag{28}$$

where $\mathbf{p}$ and $\mathbf{P}$ are the ordinary and generalized momenta. For a wave propagating on the z direction $\mathbf{A} = \mathbf{A}(z - ct)$ an averaging procedure with respect to the explicit time dependence of the Hamiltonian can be carried out. For a plane wave the time average vanishes $\langle \mathbf{A} \rangle = 0$. As a consequence under suitable conditions it can be easily shown that

$$\langle H \rangle \simeq mc^2 \left(1 + \frac{\mathbf{P}^2 + \frac{e^2}{c^2} \langle \mathbf{A}^2 \rangle}{m^2 c^2} \right)^{1/2} \tag{29}$$

This is the case in the non relativistic limit since the Hamiltonian becomes quadratic or if the vector potential has a single component $\mathbf{A} = A_y(z - ct)\, \mathbf{e}_y$. In this case supposing $p_y^2/(p_x^2 + p_z^2) \ll 1$ averaging after a first order expansion in this variable shows that (29) is still valid. As a consequence the equations of motion read

$$\frac{d\mathbf{r}}{dt} = \frac{\mathbf{P}}{\gamma\, m} \qquad \frac{d\mathbf{P}}{dt} = -\frac{e^2}{2mc^2\gamma} \operatorname{grad} \langle \mathbf{A}^2 \rangle = -\frac{mc^2}{2\gamma} \operatorname{grad} \langle \mathbf{a}^2 \rangle \tag{30}$$

The averages of generalized and ordinary momentum are the same and the gradient of the squared electromagnetic potential is the ponderomotive force in this approximation.

This force dominates when the laser pulse is circularly polarized, because the electrons heating is strongly suppressed. The features of the acceleration mechanism depend on the target geometry.

4.1 Hole Boring

For targets of thickness comparable with the pulse wavelength, we have the *hole boring* regime. The electrons density wave brakes on a distance comparable with the skin depth and the fluid approximation is no longer applicable. A piecewise constant approximation leads to a linear electric fields and the protons maximum energy can be easily evaluated. The expression one obtains is

$$E_{\max}(\mathrm{MeV}) = \frac{E_{\max}}{2mc^2} \simeq a^2\, \frac{n_c}{n} \tag{31}$$

and for an ion of charge Z the energy is multiplied by Z. The angular spread of the beam is significantly lower with respect to the TNSA acceleration but the factor n_c/n strongly reduces the energy value. Even though the scaling with a is quadratic rather than linear, only at very high values of the intensity the energy overcomes the value reached with TNSA. The only solution is to avoid the use of solid targets and work with a near critical density. This condition is naturally met for a wavelength of 10 μm since the critical density $n_c = 10^{19}$ cm^{-3} is met on gas jets. An experiment recently performed confirms that such a regime can be met and protons with a narrow energy spectrum can be accelerated [Palmer et al. (2010); Pogorelsky (2010a)].

4.2 Relativistic mirror

For ultra-thin targets of thickness comparable with the skin depth the radiation pressure is able to push all the electrons of the foil which create a huge charge separation and all the ions are promptly accelerated. The result is that the target is practically accelerated as a whole as a

rigid object behaving like a mirror whose equations of motion are

$$\frac{dx}{dt} = c\beta \qquad \frac{d\beta}{dt} = \frac{2I}{\mu c^2}\frac{1-\beta}{1+\beta}(1-\beta^2)^{3/2} \tag{32}$$

where μ is the surface density of the mirror and $I = I_0 f\left((t - x/c)/\tau_{\text{laser}}\right)$ is the laser pulse. The function $f(s)$ vanishes except for $|s| < 1$ where it is positive. The equations of motion 30 have a first integral of motion. Setting

$$t' = \frac{t}{\tau_{\text{laser}}}, \quad x' = \frac{x}{c\tau_{\text{laser}}}, \quad w = t' - x' \quad \chi = \frac{2I_0\,\tau_{\text{laser}}}{\mu\, c^2} \tag{33}$$

the equations of motion become

$$\frac{d\beta}{dt'} = \chi\, f(w)\, \frac{1-\beta}{1+\beta}\,(1-\beta^2)^{3/2} \qquad \frac{dw}{dt'} = 1-\beta \tag{34}$$

and introducing the integrating factor $C = (1+\beta)(1-\beta)^{-1}(1-\beta^2)^{-3/2}$ the differential form $dH = C\left[(1-\beta)d\beta - \chi\, f(w)\;\; (1-\beta^2)^{3/2}(1-\beta)/(1+\beta)\, dw\right]$ becomes exact and the first integral is

$$H = \chi \int_{-1}^{w} f(w')dw' - \left(\frac{1+\beta}{1-\beta}\right)^{1/2} \tag{35}$$

The initial condition corresponds to $w = -1,\ \beta = 0$ so that $H = -1$. At the end of the pulse we have $w = 1$ and $\beta = \beta_*$ which is the highest speed value. Denoting by $F = \int_{-1}^{1} f(w)dw$ the fluence we have $\chi F - [(1+\beta_*)/(1-\beta_*)]^{1/2} = -1$. We obtain β_* and γ_* as a function of $\alpha = \chi\, F$ which is given by

$$\alpha = \chi F = \frac{2I_0\, F\, \tau_{\text{laser}}\; S}{\mu\, c^2\; S} = \frac{2E_{\text{laser}}}{E_{\text{rest mirr}}} \tag{36}$$

Expressing $\gamma_* = (1-\beta_*^2)^{-1/2}$ as a function of α we obtain the expression for the kinetic energy of the ion which is given by

$$E_{\text{max}} = Am_pc^2(\gamma_* - 1) = Am_pc^2\frac{\alpha^2}{2+2\alpha} = \frac{E_{\text{laser}}}{N}\,\frac{\alpha}{1+\alpha} \tag{37}$$

where (36) has been used taking into account $E_{\text{rest mirr}} = NAm_pc^2$ where N is the number of ions in the mirror. As a consequence the efficiency of the acceleration process is given by

$$\eta = \frac{E_{\text{mirr}}}{E_{\text{laser}}} = \frac{\alpha}{1+\alpha} \tag{38}$$

From equation (36) it appears that the thinner is the mirror the higher is the efficiency and the protons energy because $\mu = AZ^{-1}\, m_p\, h\, n$. However a limit is imposed by the transparency limit Macchi et al. (2009). The target remains opaque and is accelerated as a mirror provided that

$$a \leq \zeta = \pi\frac{n}{n_c}\,\frac{h}{\lambda} \tag{39}$$

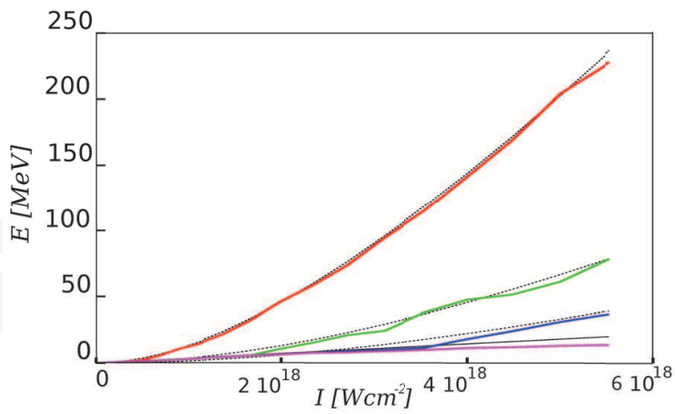

Fig. 5. Protons energy in MeV versus intensity for a pulse with $\lambda = 10\mu$m. various foil thickness are considered: $\ell = 5\mu$m (red), $\ell = 10\mu$m (green), $\ell = 15\mu$m (Blue), $\ell = 30\mu$m (purple). The 1D PIC results are compared with the analytical results for the RPA hole boring (solid black line) and the relativistic mirror (dotted line).

where n denotes the electrons density. The number N of ions in the target and the minimum number N_* below which transparency is induced and the corresponding minimum thickness h_* of the target are given by

$$N = \frac{n}{Z} h\, S = \frac{S}{Z}\ \frac{\zeta}{\lambda r_c} \qquad N_* = \frac{S}{Z}\ \frac{a}{\lambda r_c} \qquad h_* = \frac{N_*}{n\, S} = \frac{a}{Z\, \lambda\, r_c\, n_e} \tag{40}$$

In this regime, keeping the ratio h/λ fixed, the volume of the accelerated ions increases as λ^3, their number as λ if n/n_c is also kept fixed. As a consequence, at the transparency limit the parameter a and the laser power have a fixed value. The parameter α is constant if the energy is kept proportional to λ. In this case the total energy and the proton number increase with λ, whereas the energy of each proton does not vary. If the laser energy and the pulse duration both increase with λ the power remains constant. In Figure 5 we compare the analytic scaling provided by equations (31) and (37) with 1D PIC simulations for a circularly polarized 10μm pulse. The transition between these regimes is evident and the agreement between the analytical and numerical result is quite good. The RPA regime is well suited for CO_2 lasers because the native polarization is circular. Slightly overcritical targets are provided by gas jets and in the hole boring regime the choice $n \simeq n_c$ is necessary in order to achieve high energies, according to (31). In addition a quasi monochromatic spectrum is obtained at moderate intensities typical of CO_2 lasers. In this case the hole boring scenario is the most promising as recent experiments have shown [Palmer et al. (2010); Pogorelsky (2010a)].

The relativistic mirror model is very attractive on the basis on the analytical results obtained from the 1D model. However 2D and 3D simulations show that a deterioration occurs when the dimensionality is increased, due to the onset of Rayleigh-Taylor like instabilities. Considering also the difficulties met in the preparation of ultrathin targets in order to be close to the transparency limit and the requirements on the contrast, this regime is not likely to be interesting for application, even using long wavelength pulses, in a near future.

5. Near critical targets

The acceleration of protons on targets with a nearly critical electron density has been recently investigated on several experiments and PIC simulations. Positive features of this type of targets are a better efficiency in the energy transfer from the laser to the electrons and the absence of debris since the medium is transparent. The optimal length of the target is a few times the length of the laser pulse which drills a channel and accelerates longitudinally the electrons which create a magnetic field circulating around the beam axis. The magnetic field moves behind the laser pulse until it exits in the vacuum where it expands; the electrons, whose energy is dissipated, are displaced by the magnetic field and create a quasi static electric field. The ions coming from the filament around the axis are accelerated and collimated. More specifically the mechanism controlling the proton acceleration is provided by the formation of a slowly evolving magnetic dipole (a toroidal configuration in 3D geometry) behind the leading laser pulse. This structure is generated by the coherent return axial current due to the accelerated electron beam, which contains a large fraction of the laser pulse energy. The magnetic vortex, when exiting on a low density (or a vacuum) region, expands symmetrically thus creating a strong induction axial electric field. At higher electron density $n_c < n < 3n_c$ this mechanism is the most effective in the acceleration process. At lower density $n < n_c$, a significant contribution comes also from the electrostatic field due to charge separation at the channel rear side, much alike the TNSA regime.

The maximum energy of protons depends on the target thickness and density and a scaling law is obtained by equating the laser energy to the electrons energy, following the waveguide model, provided that the length of the plasma channel h is much larger than the length of the laser pulse $h \gg L_p$ to insure that the depletion of the laser energy is complete. Using equation (15), $I = a^2\, mc^3 n_c$, the laser energy in a channel reads

$$E_{\text{laser}} = \pi R^2\, \tau I = \pi R^2 L_{\text{laser}}\, a^2\, mc^2\, n_c \tag{41}$$

The electrons energy is given by

$$E_{\text{el}} = \pi R^2\, h\, n\, a\, mc^2 \tag{42}$$

and equating the energies we obtain

$$a \sim \frac{nh}{n_c L_{\text{laser}}} \tag{43}$$

Another scaling provides the optimal channel length which is given by

$$n \sim h^{3/2} \tag{44}$$

If the transition to the vacuum is not abrupt but the target with electron density n and length h continues with a decreasing density before reaching the vacuum, some improvements on the top energy and the collimation can be obtained. The main advantages with respect to the TNSA regime are that the energies reached are two or three times higher, the collimation is improved and the efficiency is higher. For wavelength in the micron range the problem is to find the right targets. This is solved naturally for pulses with wavelength in the 10 μm range, since gas jets can be used. Indeed promising results have been obtained in recent experiments. We have performed several 2D and 3D PIC simulations of quasi critical targets. The electrons

and protons density at two different times exhibiting the formation of the channel are shown in figures 6 and 7 for a 3D simulation. The spectrum of the protons is still exponential and

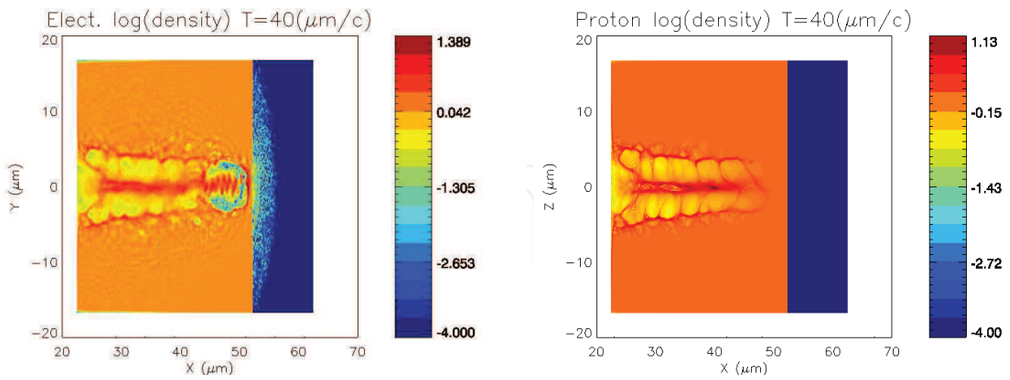

Fig. 6. Electrons (left frame) and protons (right frame) density in the case of a laser pulse of 200 TW, with wavelength $\lambda = 0.8\,\mu$m, pulse duration $\tau = 25$ fs and $a = 32$, incident on a target 30 μm thick of density $n = n_c$ at time $t = 40\mu/c$ from the the beginning of the laser target interaction. The simulation is 3D.

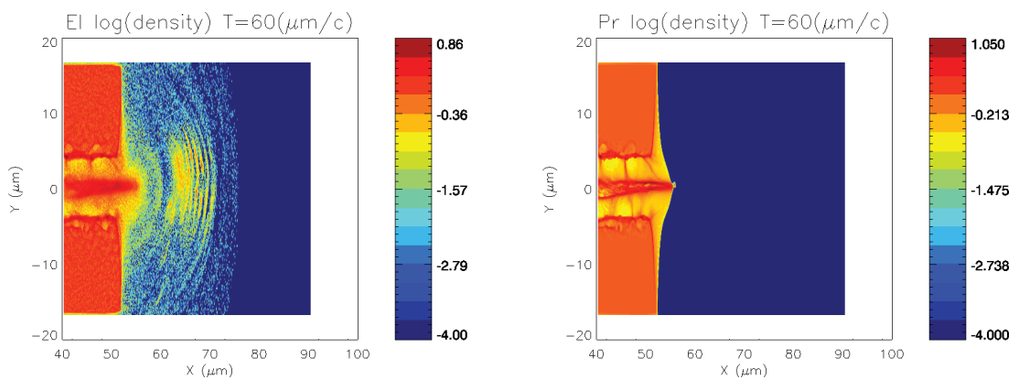

Fig. 7. The same as figure 6 at time $t = 60\mu/c$

the angular dispersion is better than for TNSA. In figure 8 we show the energy spectrum for a 200 TW laser pulse, the same as for figures 6 and 7. When a target is slightly overcritical it is transparent if the intensity is high enough. Indeed one has to take into account the self induced transparency since the critical density becomes

$$n_c = \frac{\pi}{\lambda^2 r_c}\gamma \simeq \frac{\pi}{\lambda^2 r_c}\, a \tag{45}$$

As a consequence by increasing the intensity the medium becomes transparent and the laser drills a channel. If the intensities are moderate this effect is small and a medium at a few times the critical density remains opaque and the hole boring acceleration prevails. Using a CO_2 laser with a gas jet one can have both regimes. By increasing the density at a fixed intensity the medium looses its transparency and the highest protons energy decreases reaches a minimum and then increases because the RPA hole boring regime sets in [Willingale (2009)].

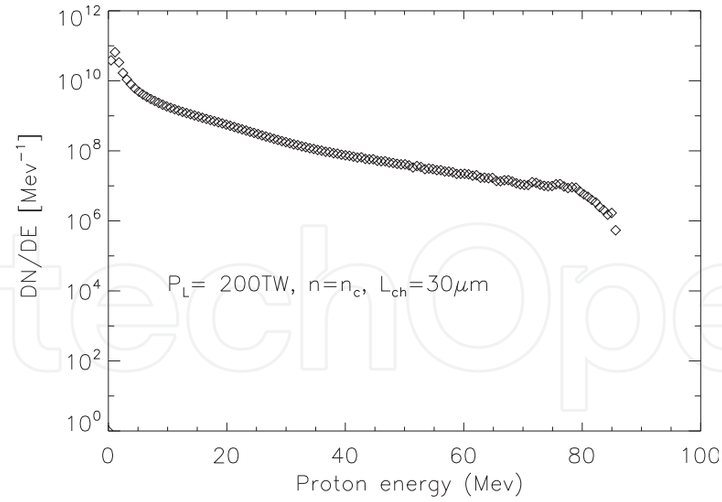

Fig. 8. Energy spectrum for a target at critical density for a laser pulse with $W = 200$ TW for the same parameters as figures 6

6. The transport

The use of protons or ions beams for medical therapy has to face severe constraints, which are not yet met by present laser produced ion bunches. Indeed the energy range is $60 \leq E \leq 250$ MeV, the average overall dose is 60 Gray (1 Gy corresponds to 1 mJ per gram) and the full dose delivery is reached in several treatments. Assuming that the dose for a single proton session is 10 Gy and that it is delivered in 2 minutes with 10 Hz pulses, the number of protons per shot to reach this dose on a 1 g tissue would be 10^6. For a TNSA beam with a maximum energy slightly above 60 MeV, such an intensity is not easily achievable because the energy spectrum is exponential and the average energy is much lower (1/7 in 3D simulations) than the maximum energy. The situation for beams obtained from the interaction with a quasi critical target is more favorable, since the collimation is better and the maximum energy is higher. The energy currently reached with compact Ti:Sa lasers are around 20 MeV. This value has been recently overcome with a CO_2 laser working with a gas target, where a monochromatic protons bunch was produced. As a consequence, presently the conditions to use for therapy the proton beams accelerated by compact high repetition lasers are not yet met. The increase of power from 100-200 TW to 1 PW is likely to allow to reach the threshold of 60 MeV of maximum energy for therapeutic use even though the intensity might be lower than required.

A possible alternative consists in maintaining the energy in the 10-30 MeV range and post-accelerating the beam. Suitable devices have already been developed to accelerate a proton beam coming from a cyclotron in this energy range. The injection energy varies from 10 MeV for a rather large DTL device [Antici (2011)] to 30 MeV for compact high field linacs like ACLIP [Amaldi et al. (2009)]. Preliminary experiments and some simulations have been already carried out. The injection of a beam in a RF cavity at 1 Hz for monochromatizing it has been experimentally proved even though at low energy (2 MeV) [Nishiuchi (2010)]. Several experiments on beam transport have been performed using quadrupoles or solenoids to focus it. A beam with $E \leq 14$ MeV has been transported through a line formed by two collimators and two permanent magnetic quadrupoles [Schollmeier (2008)]. An experiment

of transport was performed with a proton bunch accelerated by the laser PHELIX with an energy spectrum up to 30 MeV using quadrupoles or a solenoid, which proved to keep the emittance to a lower value [Hofmann (2009; 2011)]. A proposal was made for a 100 MeV device capable of delivering 10^5 protons per shot on the tissues starting from a 300 TW laser beam and $a = 60$ so that a dose of 40 Gy could be delivered on a target tissue of 0.03 g in 2 minutes at 10 Hz [Sakaki et al. (2009)] using a gantry with quadrupoles and bending magnets. Radiobiology experiments were carried out on cancer cells irradiating them with proton bunches of 0.8-2.4 MeV, obtained from laser accelerations, and the break-up of DNA double strands was observed [Yogo (2009)]. A design study for post-acceleration of a 10 MeV beam into a DTL was carried out showing that with a moderate power laser $W \leq 100$ TW and the use of microlenses right after the interaction region an injectable beam with parameters suitable for therapy could be obtained [Antici (2011)]

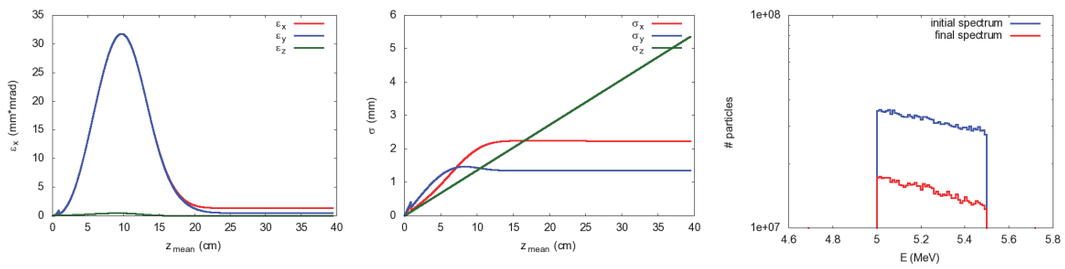

Fig. 9. Left frame: emittances ϵ_x (red), ϵ_y (blue) and ϵ_z (green) for a beam produced with a 30 TW laser pulse transported through an iris with $r = 0.5$ mm and a solenoid, starting right after the iris, of 11.7 cm, $B = 10$ Tesla and $\lambda = 2$ cm, where the B field is described by a function like $B(z) = 1/(1 + e^{-z/\lambda})$. An energy cut is set at $5 < E < 5.5$ MeV. Middle frame: envelopes σ_x (red), σ_y (blue) and σ_z (green). Right frame: initial (blue) and final (red) energy spectra. The laser has the same parameters as figure 2.

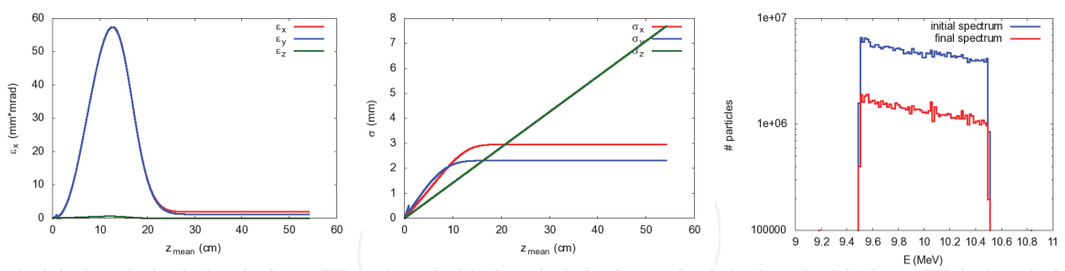

Fig. 10. Left frame: emittances ϵ_x (red), ϵ_y (blue) and ϵ_z (green) for a beam produced with a 30 TW laser pulse transported through an iris with $r = 0.5$ mm and a solenoid, starting right after the iris, of 15.6 cm, $B = 10$ Tesla and $\lambda = 2$ cm. An energy cut is set at $9.5 < E < 10.5$ MeV. Middle frame: envelopes σ_x (red), σ_y (blue) and σ_z (green). Right frame: initial (blue) and final (red) energy spectra

We have simulated the transport of a proton beam produced with a 30 TW laser pulse having a waist of 3 μm so that $I = 2\,10^{20}$ W/cm^2 and $a \simeq 10$. The simulated target was 0.5 μm thick, orthogonal to the z propagation axis, with $n = 40n_c$, with a 2 μm coating with $n = 2n_c$ and a 50 nm layer of contaminants with $n = 9n_c$ on the opposite side. The maximum energy was ~ 14 MeV. We have placed a collimator formed by a screen with a hole of 0.5 mm radius at 1 cm from the interaction region followed by a solenoid.

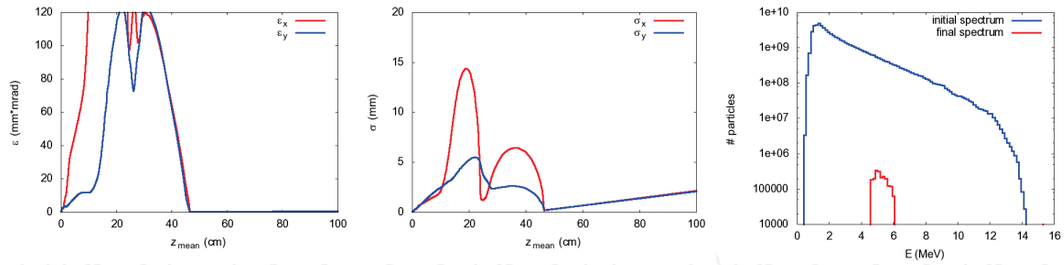

Fig. 11. Left frame: emittances ϵ_x (red) and ϵ_y (blue) for a beam produced with a 30 TW laser pulse transported through a chicane (selecting around 5 MeV), an iris with $r = 0.5$ mm and a solenoid, starting right after the iris, of 11.7 cm, $B = 10$ Tesla and $\lambda = 2$ cm. Middle frame: envelopes σ_x (red) and σ_y (blue) Right frame: initial (blue) and final (red) energy spectra

In figure 9 we show the emittance and the envelope for a small fraction of the bunch, with a cut in the energy spectrum between 5 and 5.5 MeV. We have considered also the transport of the fraction of the beam with an energy between 9.5 MeV and 10.5 MeV. The results are comparable and the emittance and envelopes are shown in Figure 10. An energy selection can be made with a physical device such as a chicane or an RF cavity to achieve the rotation in the longitudinal phase space. The chicane applied to the full bunch leads to an emittance growth along the axis where the dipoles bend the beam. By applying suitable collimators the emittance and envelopes can be reduced to reasonable values but only a small fraction of the beam reaches the end of the transport line. In Figure 11, we show the full bunch propagating along a chicane and then focusing in a solenoid with field of $B = 10$ Tesla.

Other more effective methods based on selection of particles at the desired energy by putting collimator at the corresponding focus point of a solenoid are under investigation.

No transport experiments have been performed with CO_2 laser accelerated proton beams, but the situation is certainly much more favorable if a quasi-monochromatic peak can be obtained with adequate intensity [Haberberger, Tochitsky, Fiuza, Gong, Fonseca, Silva, Mori & Joshi (2011); Haberberger, Tochitsky, Gong & Joshi (2011)]. In this case no energy selection is required and the transport on the beam becomes quite easy because tight focusing can be achieved preventing emittance increase and keeping the beam size to small values suitable for injection in a linac.

7. Conclusions: Protons and ions therapy

Cancer treatment, a priority for health care in advanced countries, is based on surgery, chemo-therapy and radiation therapy. Early detection of tumors increases the survival period but there are limits to massive and frequent screening. Unlike chemotherapy radiation therapy killing of malignant cells is quite homogeneous and can be effective even for massive tumors. The most common treatment is based on X rays, driven by electron accelerators. The reason is compactness of the accelerating device and moderate cost, affordable by medium size hospitals. However most of ionizing radiations, including X rays, exhibit a peak in dose deposition close to the entry point and a subsequent exponential decay. As a consequence the dose deposition in healthy tissues is important, even when this undesirable effect is minimized by irradiating from different directions and modulating the intensity (IMRT). The dose deposition mechanism for protons and ions is different and the dose curve as function

of depth exhibits a sharp peak, known as Bragg peak. Healthy tissues are spared and this therapy is applicable to the most severe cases which are not suitable for surgery. The protons are usually accelerated by cyclotrons and a large gantry is needed to rotate the beam around the patient. Carbon ions are accelerated by synchrotrons, which have a larger size, require heavy transport lines and a very large gantry. Even though the number of centers for protons and ions therapy is increasing they are up to now limited to national facilities. A reduction of size and cost of a protons accelerator for therapy would allow the creation of regional centers extending this treatment to a larger fraction of patients. Devices based on innovative techniques such as the superconducting cyclotron or the dielectric wall accelerator have been proposed but conclusive results have not yet been achieved. Laser acceleration of protons has entered this competition even though several years are needed before the feasibility is actually demonstrated. The typical dose for therapy is 60 Gy which means 60 mJ on a mass of 1 g. Split over 6 session this amounts to 10 mJ and corresponds to 10^9 protons of 60 MeV which is the threshold for very superficial tumors. Supposing each bunch contains 10^6 protons at 10 Hz repetition rate this dose is delivered in a couple of minutes. The major problem is that the energy and intensity required can hardly be reached with compact existing Ti:Sa lasers. Suppose that a bunch of 10^{12} protons is accelerated by TNSA having an average energy of 10 MeV and maximum energy of 70 MeV, according to previous scaling, then the total proton energy is 1.6 J and supposing a 10% efficiency the laser energy would be 16 J. Since the spectrum is exponential the fraction of protons at 60 MeV with $\Delta E/E = 1\%$ would be $1.5\,10^8$. This is a very demanding requirement on the laser. If we choose instead an average energy of 5 MeV we would have the same number of protons at an energy of 30 MeV, for the same $\Delta E/E$.

After post-acceleration one could reach not only the 60 MeV threshold but also higher energies, suitable for deep tumors.

The real problem with TNSA or improved TNSA, achieved with a foam deposition at quasi critical density on the illuminated surface, is that the protons having the desired energy are a very small fraction of the total and carry out a very small fraction of the total energy. Increasing the repetition rate form 10 to 100 Hz would help but would not solve the problem. The way out is to produce a quasi monochromatic spectrum. This has been achieved with a CO_2 laser on a gas jet and this result is of extreme interest. The use of ultrathin nanometric targets allows to obtain quasi monochromatic beams via RPA, but in spite of the scientific interest this regime is still very far out from possible applications due to the the extremely high contrast required on the laser beam. The use of gas targets and a suitably shaped beam pulse seem to be the corner stones in the production of a quasi monochromatic beam. In this respect the CO_2 laser beams have an advantage with respect to pulses of shorter wavelength. For a quasi monochromatic beam the intensity is still rather low because only a small fraction of the laser energy is transferred to the beam. Once the energy and intensity requirements are satisfied other conditions have to be satisfied to render the proton beam suitable for therapy: the shot to shot stability must be kept within a narrow range and suitable dose control systems have to be developed [Linz & Alonso (2007)]. As a consequence it will take several years before laser accelerators can meet the requirements for clinical use. During this period the laser performance will be improved, new targets will be developed, transport and post acceleration systems will be tested and beam quality and stability will be pursued. Even though most of the research activity will be devoted to short wavelength lasers, the

development of long wavelength system such as CO_2 lasers will hopefully continue because they may provide a very valuable alternative and solve some of the most critical problems such as monochromaticity and proton beam quality.

8. Acknowledgments

We would like to thank the Italian Ministry of Foreign Affairs (MAE) for a grant we received for the scientific cooperation with Japan to develop the research project PROMETHEUS, devoted to a research infrastructure on laser driven proton sources for biomedical applications. We thank the Fondazione del Monte di Bologna e Ravenna for a grant devoted to the feasibility study of a hybrid accelerator devoted to biomedical Research within the framework of PROMETHEUS. We acknowledge the Alma Mater Foundation for the governance of the PROMETHEUS project.

9. References

Amaldi, U., Braccini, S. & Puggioni, P. (2009). High frequency linacs for hadrontherapy, *Reviews of Accelerator Science and Technology* 2(111131).

Antici, P. (2011). A compact post-acceleration scheme for laser-generated protons, *Physics of Plasmas* 18.

Benedetti, C., Sgattoni, A., Turchetti, G. & Londrillo, P. (2008). Aladyn: A high accuracy pic code for the maxwell-vlasov equations, *IEEE Transactions on Plasma Science* 36(4).

Bulanov, S. (2008). Accelerating protons to therapeutic energies with ultraintense, ultraclean, and ultrashort laser pulses, *Medical Physics* 35.

Bulanov, S. S. (2010). Generation of gev protons from 1pw laser interaction with near critical density targets, *Physics of Plasmas* 17(043105).

Fukuda, Y. & Bulanov, S. (2009). Energy increase in multi-mev ion acceleration in the interaction of short laser pulse with a cluster gas target, *Phys. Rev. Letters* 103(165002).

Haberberger, D., Tochitsky, S., Fiuza, F., Gong, C., Fonseca, R. A., Silva, L. O., Mori, W. B. & Joshi, C. (2011). Collisionless shocks in laser-produced plasma generate monoenergetic high-energy proton beams, *Nature Physics* .

Haberberger, D., Tochitsky, S., Gong, C. & Joshi, C. (2011). Production of 25 mev protons in co_2 laser plasma interactions in a gas jet, *Proceedings of 2011 Particle Accelerator Conference, New York, NY, USA* .

Henig, A. (2009). Radiation-pressure acceleration of ion beams driven by circularly polarized laser pulses, *Phys. Rev. Lett.* 103(245003).

Hofmann, I. (2009). Laser accelerated ions and their potential for therapy, *Proceedings of HIAT09, Venice, Italy* .

Hofmann, I. (2011). Collection and focusing of laser accelerated ion beams for therapy applications, *Phys. Rev. Spec. Top. Acc. and Beams* 14(031304).

Leemans, W. P., Nagler, B., Gonsalves, A. J., Tóth, C., Nakamura, K., Geddes, C. G. R., Esarey, E., Schroeder, C. B. & Hooker, S. M. (2006). Gev electron beams from a centimetre-scale accelerator, *Nature Physics* 2: 696–699.

Linz, U. & Alonso, J. (2007). What will it take for laser driven proton accelerators to be applied to tumor therapy, *Phys. Rev. Special Topics Accel. and Beams* 10(094801).

Londrillo, P., Benedetti, C., Sgattoni, A., Turchetti, G. & Lucchio, L. D. (2010). Comparison of scaling laws with pic simulations for protons accelerated with long wavelength pulses, *Nucl. Instr. and Meth. in Phys. Res. A* 620: 51–55.

Londrillo, P., Sgattoni, A., Sumini, M. & Turchetti, G. (2011). Optical acceleration and perspectives for cancer therapy with proton beams, *Proceedings del workshop OSCM - Oncogenesi tra scienza e clinica medica - Frascati 10-11 giugno 2010 - ENEA report* .

Macchi, A., Cattani, F., Liseykina, T. V. & Cornolti, F. (2005). Laser acceleration of ion bunches at the front surface of overdense plasmas, *Phys. Rev. Lett.* 94(165003).

Macchi, A., Veghini, S. & Pegoraro, F. (2009). Light sail acceleration reexamined, *Phys. Rev. Lett.* 103(085003).

Melone, J. J. (2011). In situ characterisation of permanent magnetic quadrupoles for focussing proton beams.
URL: *http://arxiv.org/abs/1104.1932v1*

Mourou, G. A., Tajima, T. & Bulanov, S. V. (2006). Optics in the relativistic regime, *Rev. of Mod. Physics* 78: 309–371.

Murakami, M. (2008). Radiotherapy using a laser proton accelerator.
URL: *http://arxiv.org/abs/0804.3826*

Nakamura, T., Bulanov, S., Esirkepov, T. & Kando, M. (2010). High-energy ions from near-critical density plasmas via magnetic vortex acceleration, *Phys. Rev. Lett.* 105(135002).

Nakamura, T., Tampo, M., Kodama, R., Bulanov, S. V. & Kando, M. (2010). Interaction of high contrast laser pulse with foam-attached target, *Physics of Plasmas* 17(113107).

Naumova, N. M. & Bulanov, S. V. (2002). Polarization and anisotropy in three dimensional relativistic self focusing, *Physical Review E* 65(045402).

Nishiuchi, M. (2010). Measured and simulated transport of 1.9 mev laser-accelerated proton bunches through an integrated test beam line at 1 hz, *Phys. Rev. Spec. Top. Acc. and Beams* 13(071304).

Noda, A. (2008). Quality improvement of laser produced protons by phase rotation and its possible exyension to high energies, *Proceedings of LINAC08, Victoria, BC, Canada* .

Palmer, C. A. J., Dover, N. P., Pogorelsky, I., Babzien, M., Dudnikova, G. I., Ispiriyan, M., Polyanskiy, M. N., Schreiber, J., Shkolnikov, P., Yakimenko, V. & Najmudin, Z. (2010). Monoenergetic proton beams accelerated by a radiation pressure driven shock.
URL: *http://arxiv.org/abs/1006.3163*

Passoni, M. & Lontano, M. (2004). One dimensional model of the electrostatic ion acceleration in altradense laser-solid acceleration, *Laser and particle beams* 22.

Pogorelsky, I. V. (2010a). Laser energy conversion to solitons and monoenergetic protons in near critical hydrogen plasma, *Proceedings of IPAC10, Kyoto, Japan* .

Pogorelsky, I. V. (2010b). Ultrafast co_2 laser technology. application to ions acceleration, *NIM A* 620: 67–70.

Sakaki, H., Hori, T., Nishiuchi, M., Bolton, P., Daido, H., Kawanishi, S., Sutherland, K., Souda, H., Noda, A., Iseki, Y. & Yoshiyuki, T. (2009). Designing integrated laser-driven ion accelerator systems for hadron therapy at pmrc (photo medical research center), *Proceedings of the 23rd Particle Accelerator Conference, Vancouver, Canada* .

Schollmeier, M. (2008). Controlled transport and focusing of laser-accelerated protons with miniature magnetic devices, *PRL* 101(055004).

Snavely, R. A. (2000). Intense high-energy proton beams from petawatt-laser irradiation of solids, *PRL* 85: 2945–2948.

Tajima, T. & Dawson, J. M. (1979). Laser electron accelerator, *Phys. Rev. Lett.* 43(4): 267–270.

Willingale, L. (2009). Characterization of high intensity laser propagation in the relativistic transport regime through measurements of energetic proton beams, *PRL* 102(125002).

Yogo, A. (2008). Laser ion acceleration via control of the near-critical density target, *Phys. Rev. E* 77(016401).

Yogo, A. (2009). Application of laser-accelerated protons to the demonstration of dna double-strand breaks in human cancer cells, *Appl. Phys. Lett.* 94(181502).

Zani, A., Sgattoni, A. & Passoni, M. (2011). Parametric investigations of target normal sheath acceleration experiments, *Nuclear Instruments and Methods in Physics Research A* 653: 94–97.

Zeil, K., Kraft, S. D., Bock, S., Bussmann, M., Cowan, T. E., Kluge, T., Metzkes, J., Richter, T., Sauerbrey, R. & Schramm, U. (2010). The scaling of proton energies in ultrashort pulse laser plasma acceleration, *New Journal of Physics* 12(045015).

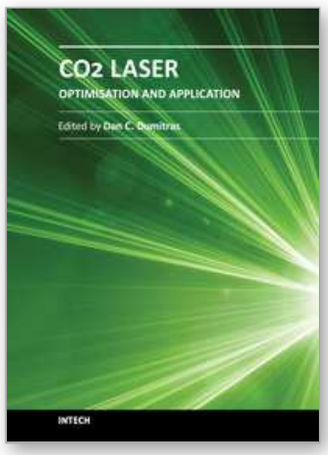

CO2 Laser - Optimisation and Application
Edited by Dr. Dan C. Dumitras

ISBN 978-953-51-0351-6
Hard cover, 436 pages
Publisher InTech
Published online 21, March, 2012
Published in print edition March, 2012

The present book includes several contributions aiming a deeper understanding of the basic processes in the operation of CO2 lasers (lasing on non-traditional bands, frequency stabilization, photoacoustic spectroscopy) and achievement of new systems (CO2 lasers generating ultrashort pulses or high average power, lasers based on diffusion cooled V-fold geometry, transmission of IR radiation through hollow core microstructured fibers). The second part of the book is dedicated to applications in material processing (heat treatment, welding, synthesis of new materials, micro fluidics) and in medicine (clinical applications, dentistry, non-ablative therapy, acceleration of protons for cancer treatment).

INTECH
open science | open minds

InTech Europe
University Campus STeP Ri
Slavka Krautzeka 83/A
51000 Rijeka, Croatia
Phone: +385 (51) 770 447
Fax: +385 (51) 686 166
www.intechopen.com

InTech China
Unit 405, Office Block, Hotel Equatorial Shanghai
No.65, Yan An Road (West), Shanghai, 200040, China
中国上海市延安西路65号上海国际贵都大饭店办公楼405单元
Phone: +86-21-62489820
Fax: +86-21-62489821

IntechOpen